Chapter 3

Numerical Results and Discussion

A computer program is written in FORTRAN language to evaluate the frequency equations of a laminated transversely isotropic circular cylinder. The IMSL subroutine is employed to evaluate the Bessel functions. The interval-halved iteration technique is used to search for the roots of the dispersion equations.

3.1 Roots of Frequency Equations

Note that the exact dispersion relations for some cases in section 2.7 contain the modified Bessel functions of the first kind, $I_\nu(x)$, and of the second kind, $K_\nu(x)$, where ν are integer orders of the functions and x are arguments defined in section 2.7. For $x > 0$ and $\nu \geq 0$, $I_\nu(x)$ is a positive function which increases monotonically as $x \longrightarrow \infty$, while $K_\nu(x)$ is a positive function which decreases monotonically as $x \longrightarrow \infty$. The asymptotic behavior of these functions as $x \longrightarrow \infty$ is given by (Lebedev, 1965)

$$I_\nu(x) \approx \frac{e^x}{\sqrt{2\pi x}}, \qquad x \longrightarrow \infty,$$

$$K_\nu(x) \approx \sqrt{\frac{\pi}{2x}}\, e^{-x}, \qquad x \longrightarrow \infty. \tag{46}$$

For small x the asymptotic formulas of these function are given by (Lebedev, 1965)

$$I_\nu(x) \approx \frac{x^\nu}{2^\nu \Gamma(1+\nu)}, \qquad x \longrightarrow 0,$$

$$K_\nu(x) \approx \frac{2^{\nu-1}\Gamma(\nu)}{x^\nu}, \qquad x \longrightarrow 0,$$

$$K_0(x) \approx \log\frac{2}{x}, \qquad x \to 0, \tag{47}$$

and therefore

$$I_\nu(0) = 0 \text{ if } \nu > 0,\ I_0(0) = 1, K_\nu(0) = \infty.$$

When the arguments of the modified Bessel functions are very small or very large, one of these functions is magnified while another is comparatively very small. The numerical evaluation for this case becomes inaccurate and causes singularity in the matrix $[D_k]$ in Eq. (28). Thus, instead of the modified Bessel functions, I and K, the values of $e^{-x}I$ and $e^{x}K$ are computed, in order to increase the range of computability of Bessel functions without overflow. IMSL subroutine is employed to evaluate the functions $e^{-x}I$ and $e^{x}K$. In the matrix $[D_k]$, where the values of the modified Bessel functions are required, the functions $e^{-\psi_k}I_\nu(\psi_k)$ and $e^{\psi_k}K_\nu(\psi_k)$, where ψ_k denotes the arguments of these functions at $r = r_k$, are computed instead of $I_\nu(\psi_k)$ and $K_\nu(\psi_k)$. For the matrix $[D_{k+1}]$, the functions $\frac{e^{-\psi_k}}{e^{-\psi_{k+1}}}I_\nu(\psi_{k+1})$ and $\frac{e^{\psi_k}}{e^{\psi_{k+1}}}K_\nu(\psi_{k+1})$, where ψ_{k+1} denotes the arguments of these functions at $r = r_{k+1}$, are computed instead of $I_\nu(\psi_{k+1})$ and $K_\nu(\psi_{k+1})$. It can be seen that the same column in the matrices $[D_k]$ and $[D_{k+1}]$ are multiplied by $e^{-\psi_k}$ or e^{ψ_k} depending on whether the columns of these matrices present the functions I or K. Since these multipliers are constant for each layer, they can then be absorbed in the arbitrary constants of the layer.

3.2 Numerical Results and Discussion

In this section, five numerical examples for dispersion characteristics of the free vibration of homogeneous and laminated cylinders are presented:

1. Homogeneous isotropic hollow cylinders with different H/R ratios.
2. A three-layered cylinder composed of aluminum core and boron/epoxy facings with H/R=1.0.
3. Four-layered cylinders graphite/epoxy and glass/epoxy layers with different H/R ratios.
4. A ten-layered cylinder composed of graphite/epoxy and glass/epoxy layers with H/R = 1.0.

5. Graphite/epoxy and Glass/epoxy cylinders with H/R = 1.0 and different number of layers.

The first two examples are to illustrate the accuracy and the efficiency of the propagator matrix method. The applicability of the method for thin and thick laminated cylinders are presented by the third example. The fourth example demonstrates the applicability of the method for a laminated cylinder with large number of layers. Dispersion behaviors of the first two modes of laminated cylinders having different number of layers are studied in the last example.

In all examples, the frequency and the axial wavenumber are the normalized frequency, Ω, and the normalized axial wavenumber, ζ, respectively, with the forms of:

$$\Omega = \frac{\omega}{\omega_{ref}} \quad ; \qquad \zeta = \frac{\xi}{\xi_{ref}},$$

where ω_{ref} and ξ_{ref} are the reference frequency and the reference axial wavenumber, respectively.

Example 1

The free vibrations, both axisymmetric and torsional vibrations, of infinite homogeneous isotropic hollow cylinders with the Poisson's ratio of 0.30 and 3 different H/R ratios are considered. The reference frequency and reference axial wavenumber are, respectively;

$$\omega_{ref} = \frac{\pi}{H}\sqrt{\frac{\mu}{\rho}} \quad ; \qquad \xi_{ref} = \frac{\pi}{H},$$

where μ is shear modulus, ρ is the mass density, and H is the thickness of cylinder.

The natural frequencies of three cylinders having different thickness to mean radius ratios (H/R) are investigated. The results obtained by the propagator matrix method are compared with the existing results for single layer isotropic cylinders presented by Armenakas, et al.(1969). For axisymmetric free vibration, the comparison of the numerical results of the first four modes for different cylinders are presented in Tables 3.1, 3.2, and 3.3. The results in

columns A represent the existing results and the results in columns P are those obtained by the propagator matrix method. For torsional vibration, the comparison of the first two cut-off frequencies are presented in Table 3.4.

It can be seen from Tables 3.1 to 3.4 that the results obtained by the present method and those given by Armenakas are in excellent agreement. Few discrepancies between the results are in the fifth digit. The results confirm the applicability and accuracy of the method for isotropic cylinders.

Table 3.1 The first four axisymmetric frequencies of a homogeneous isotropic hollow cylinder with H/R=0.1

ζ	Ω (Modes)							
	1st		2nd		3rd		4th	
	A	P	A	P	A	P	A	P
0.0	0.00000	0.00000	0.05387	0.05387	1.00038	1.00038	1.87168	1.87168
0.1	0.05292	0.05291	0.16977	0.16977	1.01735	1.01734	1.85054	1.85054
0.2	0.07614	0.07614	0.33744	0.33744	1.06538	1.06537	1.81272	1.81272
0.3	0.13037	0.13037	0.50369	0.50369	1.13790	1.13790	1.77809	1.77808
0.4	0.20438	0.20438	0.66702	0.66702	1.22798	1.22797	1.75261	1.75261
0.5	0.28969	0.28969	0.82550	0.82550	1.33001	1.33001	1.73966	1.73965
0.6	0.38165	0.38165	0.97626	0.97626	1.43993	1.43992	1.74265	1.74265
0.7	0.47756	0.47756	1.11496	1.11495	1.55474	1.55474	1.76612	1.76611
0.8	0.57580	0.57580	1.23613	1.23612	1.67720	1.67220	1.81546	1.81545
0.9	0.67537	0.67537	1.33571	1.33571	1.79041	1.79040	1.89443	1.89443
1.0	0.77563	0.77563	1.41484	1.41484	1.90773	1.90772	2.00141	2.00141

Table 3.2 The first four axisymmetric frequencies of a homogeneous isotropic hollow cylinder with H/R=1.0

ζ	Ω (Modes)							
	1st		2nd		3rd		4th	
	A	P	A	P	A	P	A	P
0.0	0.00000	0.00000	0.60059	0.60059	1.04127	1.04127	1.99847	1.99847
0.1	0.16029	0.16029	0.59789	0.59789	1.06120	1.06120	1.95264	1.95264
0.2	0.31307	0.31307	0.59903	0.59903	1.11577	1.11577	1.90427	1.90427
0.3	0.43816	0.43816	0.63321	0.63321	1.19482	1.19482	1.86456	1.86456
0.4	0.50838	0.50838	0.73458	0.73458	1.28993	1.28993	1.83493	1.83493
0.5	0.55369	0.55369	0.87513	0.87513	1.39566	1.39566	1.81691	1.81691
0.6	0.60347	0.60347	1.02274	1.02274	1.50855	1.50855	1.81261	1.81260
0.7	0.66352	0.66352	1.16551	1.16551	1.62631	1.62631	1.82516	1.82516
0.8	0.73297	0.73297	1.29603	1.29603	1.74708	1.74708	1.85928	1.85928
0.9	0.80978	0.80978	1.40784	1.40784	1.86743	1.86743	1.92191	1.92191
1.0	0.89200	0.89200	1.49809	1.49809	1.97696	1.97696	2.02388	2.02388

Table 3.3 The first four axisymmetric frequencies of a homogeneous isotropic hollow cylinder with H/R=1.9

ζ	Ω (Modes)							
	1st		2nd		3rd		4th	
	A	P	A	P	A	P	A	P
0.0	0.00000	0.00000	1.19078	1.19078	1.22956	1.22955	2.18355	2.18354
0.1	0.16086	0.16086	1.15497	1.15497	1.27838	1.27838	2.18575	2.18575
0.2	0.31926	0.31926	1.12022	1.12022	1.35268	1.35268	2.19254	2.19254
0.3	0.47186	0.47186	1.10396	1.10396	1.43663	1.43663	2.20440	2.20440
0.4	0.61332	0.61332	1.11232	1.11232	1.52757	1.52757	2.22214	2.22214
0.5	0.73570	0.73570	1.15285	1.15285	1.62355	1.62355	2.24687	2.24687
0.6	0.83259	0.83259	1.23078	1.23078	1.72278	1.72278	2.28002	2.28001
0.7	0.90756	0.90756	1.34049	1.34048	1.82367	1.82367	2.32324	2.32324
0.8	0.97156	0.97156	1.46815	1.46814	1.92510	1.92510	2.37822	2.37822
0.9	1.03321	1.03321	1.60139	1.60139	2.02699	2.02698	2.44624	2.44624
1.0	1.09668	1.09667	1.73159	1.73159	2.13088	2.13088	2.52757	2.52757

Table 3.4 The two cut-off torsional frequencies of a homogeneous cylinders with different H/R

H/R	Ω (Modes)			
	1^{st}		2^{nd}	
	A	P	A	P
0.10	1.00190	1.00190	2.00095	2.00095
0.30	1.01710	1.01710	2.00870	2.00870
0.50	1.04752	1.04752	2.02491	2.02491
1.00	1.18920	1.18920	2.11601	2.11601
1.50	1.40822	1.40821	2.33372	2.33372
1.90	1.59281	1.59281	2.61066	2.61066

Example 2

The axisymmetric free vibration of a three-layered transversely isotropic hollow cylinder with H/R = 1.0 is considered. The cylinder is composed of aluminum core and boron/epoxy facing where material properties of both materials are given in Appendix A. The geometry of the three layers are; $H^{(1)} = H^{(3)}$; $H^{(1)}/H^{(2)} = 0.1$. $H^{(i)}$, i = 1, 2, 3 represent the thickness of the inner, middle, and the outer layer, respectively. The reference frequency and reference axial wavenumber are, respectively;

$$\omega_{ref} = \frac{\pi}{H^{(2)}}\sqrt{\frac{C_{44}^{(2)}}{\rho^{(2)}}}; \qquad \xi_{ref} = \frac{\pi}{H^{(2)}}.$$

The results for the longitudinal vibration obtained by the present method are compared with the existing results presented by Keck and Armenakas (1971) in the form of frequency spectrum shown in Figure 3.1.

In the case of torsional vibration, two approaches are employed, viz. the direct method (detail in Appendix C), and the propagator matrix method. Comparison of results from the two methods are presented as Figure 3.2.

As seen in Figure 3.1, the results obtained by the present method and those presented by Keck and Armenakas are in excellent agreement. For torsional vibration, Figure 3.2, the results from both methods are exactly the same. This confirms the applicability and accuracy of the method for a layered transversely isotropic cylinder.

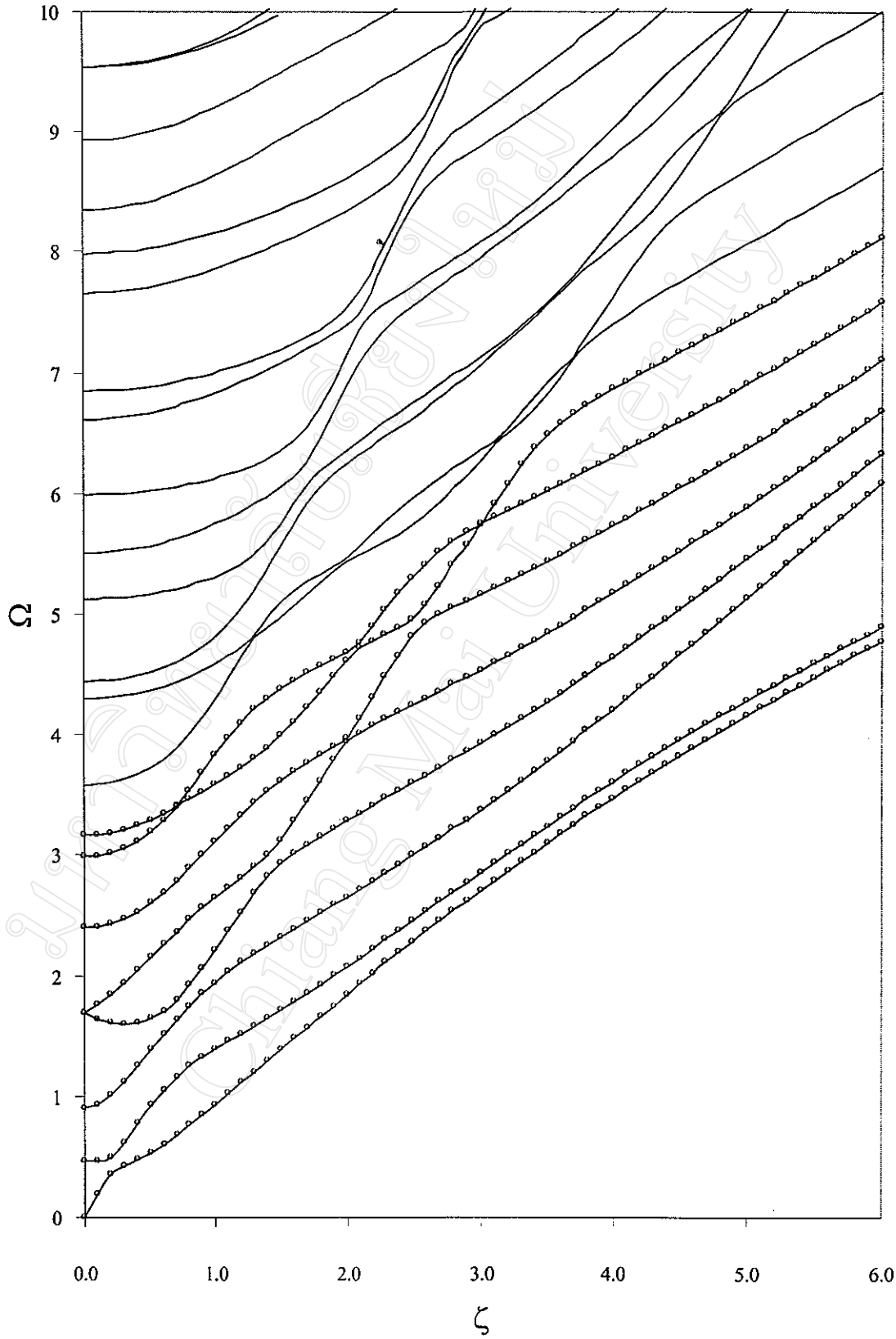

Figure 3.1 Axisymmetric frequency spectrum for a cylinder composed of aluminum core and boron/epoxy facings with H/R = 1.0 (—— propagator matrix; O Keck and Armenakas (1971))

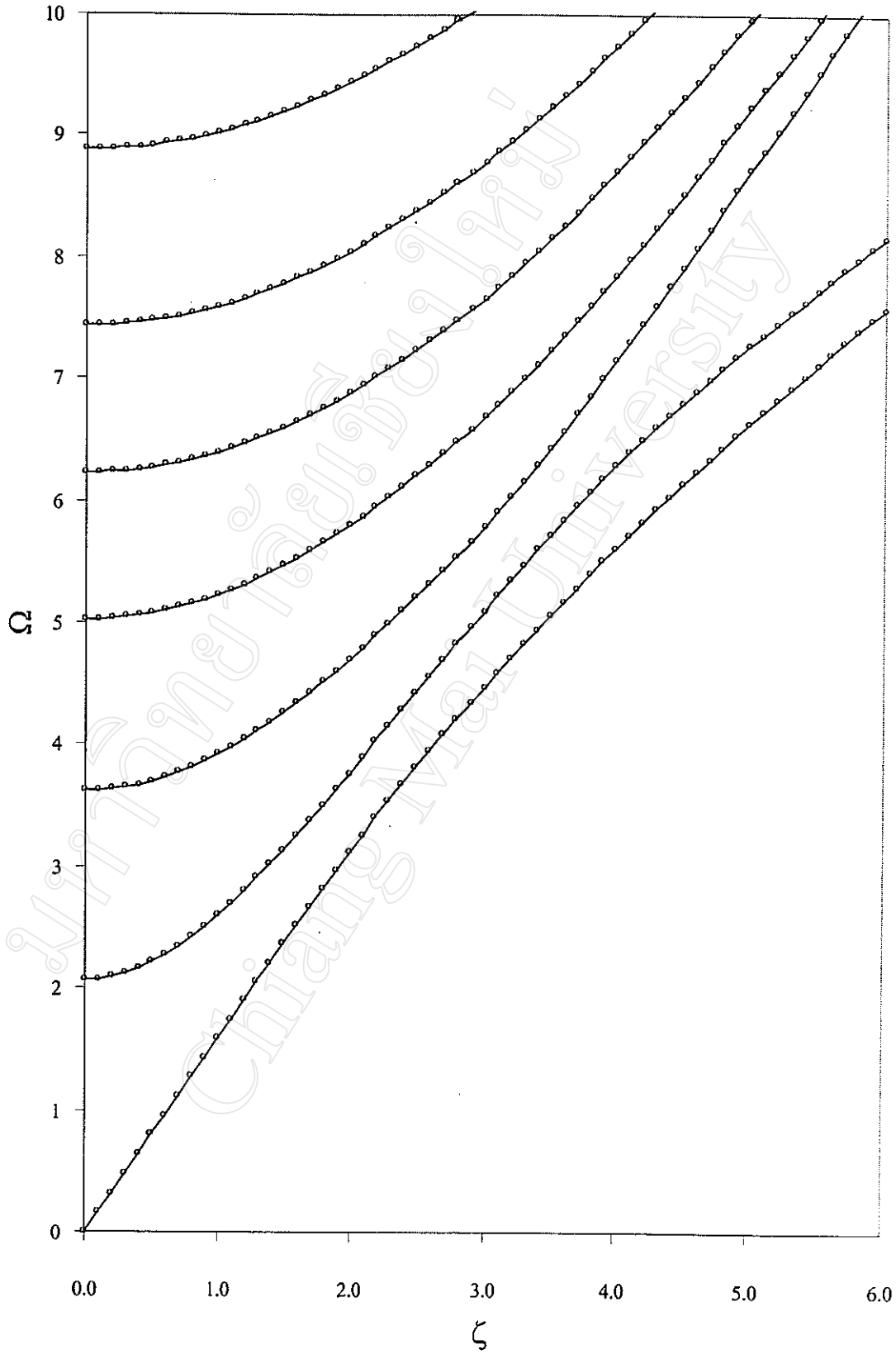

Figure 3.2 Torsional frequency spectrum for a cylinder composed of aluminum core and boron/epoxy facings with H/R = 1.0 (—— propagator matrix; O Keck and Armenakas (1971))

Example 3

The wave propagation in four-layered [Gr/Gl/Gr/Gl] laminated cylinders with H/R of 0.1, 0.5, 1.0, 1.5, and 1.9 is investigated. Gr and Gl denote graphite/epoxy and glass/epoxy, respectively. The material properties of both materials are given in Appendix A. The fiber directions are in the axial direction of the cylinders. The thickness ratio $H^{(Gr)}/H^{(Gl)}$ is 0.5. The reference frequency and the reference wavenumber are defined, respectively, as:

$$\omega_{ref} = \frac{\pi}{H}\sqrt{\frac{C_{44}^{(Gr)}}{\rho^{(Gr)}}} \quad ; \qquad \xi_{ref} = \frac{\pi}{H}.$$

Figures 3.3 to 3.7 show the frequency spectra of the cylinders. This demonstrates the applicability of the method for thin and thick cylinders. It can be seen from Figures 3.3 to 3.7 that as the H/R ratio increases, the effect of the change in H/R ratio on the dispersion characteristics become more pronounced. Two effects that can be noticed are the increase of cut-off frequencies and the change in weak coupling between modes. For comparably thin cylinders, Figures 3.3 and 3.4, the change in the H/R ratio shows no significant influence on the dispersion behavior. For moderately thick cylinders, Figures 3.4 to 3.6, the change in the H/R ratio alters the first few modes of vibration. These effects, however, are localized in low frequency and low wavenumber regions. For comparatively thick cylinders, Figures 3.6 and 3.7, the increase in the H/R ratio increases the cut-off frequencies considerably and switches the weak coupling modes.

Although the change in H/R ratio has the aforementioned effects on the dispersion characteristics, it can be seen from Figures 3.3 to 3.7 that normalized wave velocity, the ratio of $\frac{\Omega}{\zeta}$, for each mode remain the same at high frequencies.

The effects of the change in the H/R ratio for torsional case are different than those for longitudinal vibration. For torsional vibration, the increase of the H/R ratio elevates each spectrum, except for comparatively thin cylinders, Figures 3.3 and 3.4.

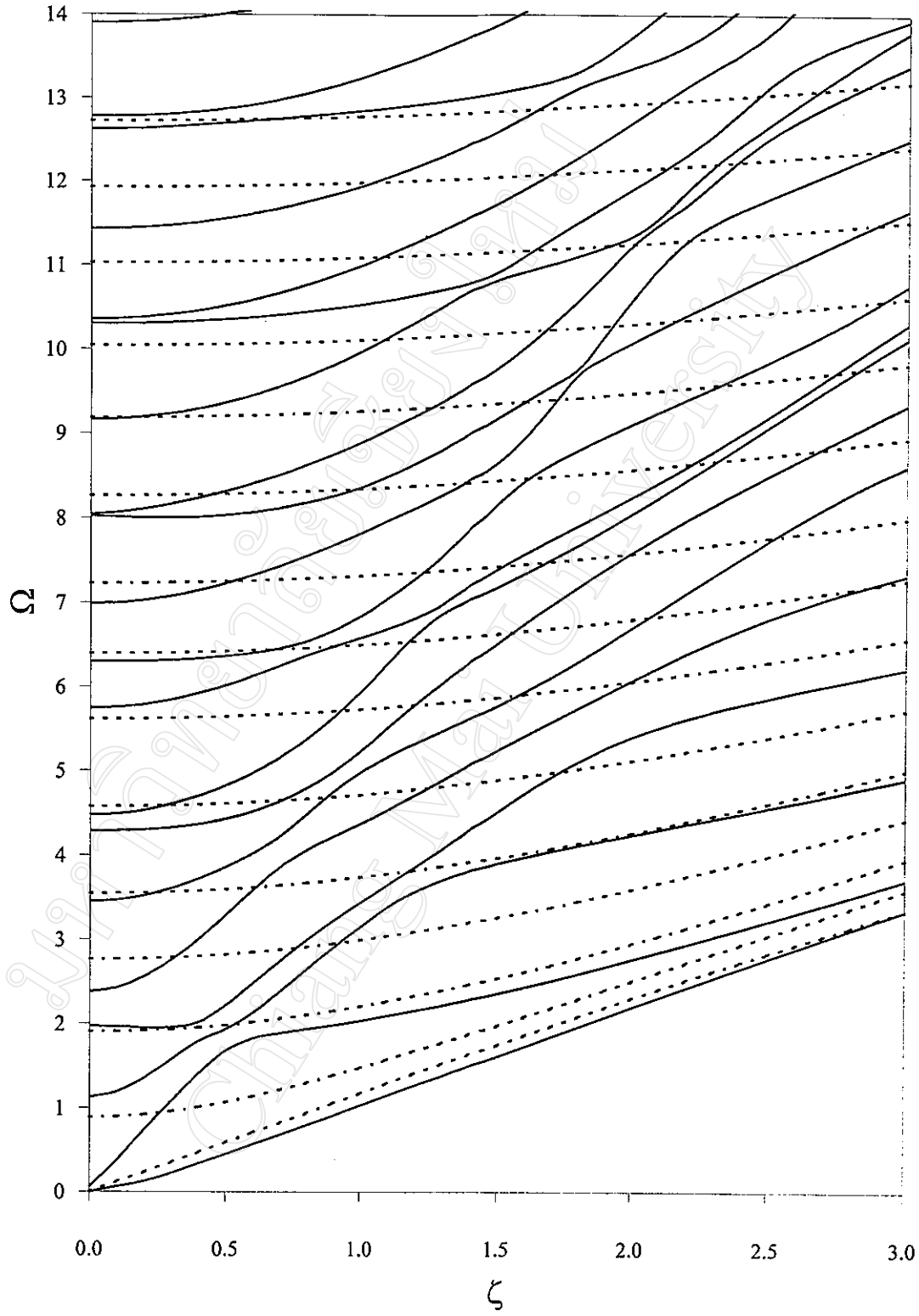

Figure 3.3 Frequency spectrum for a cylinder composed of [Gr/Gl/Gr/Gl] with H/R = 0.1 (—— Longitudinal mode, ----- Torsional mode)

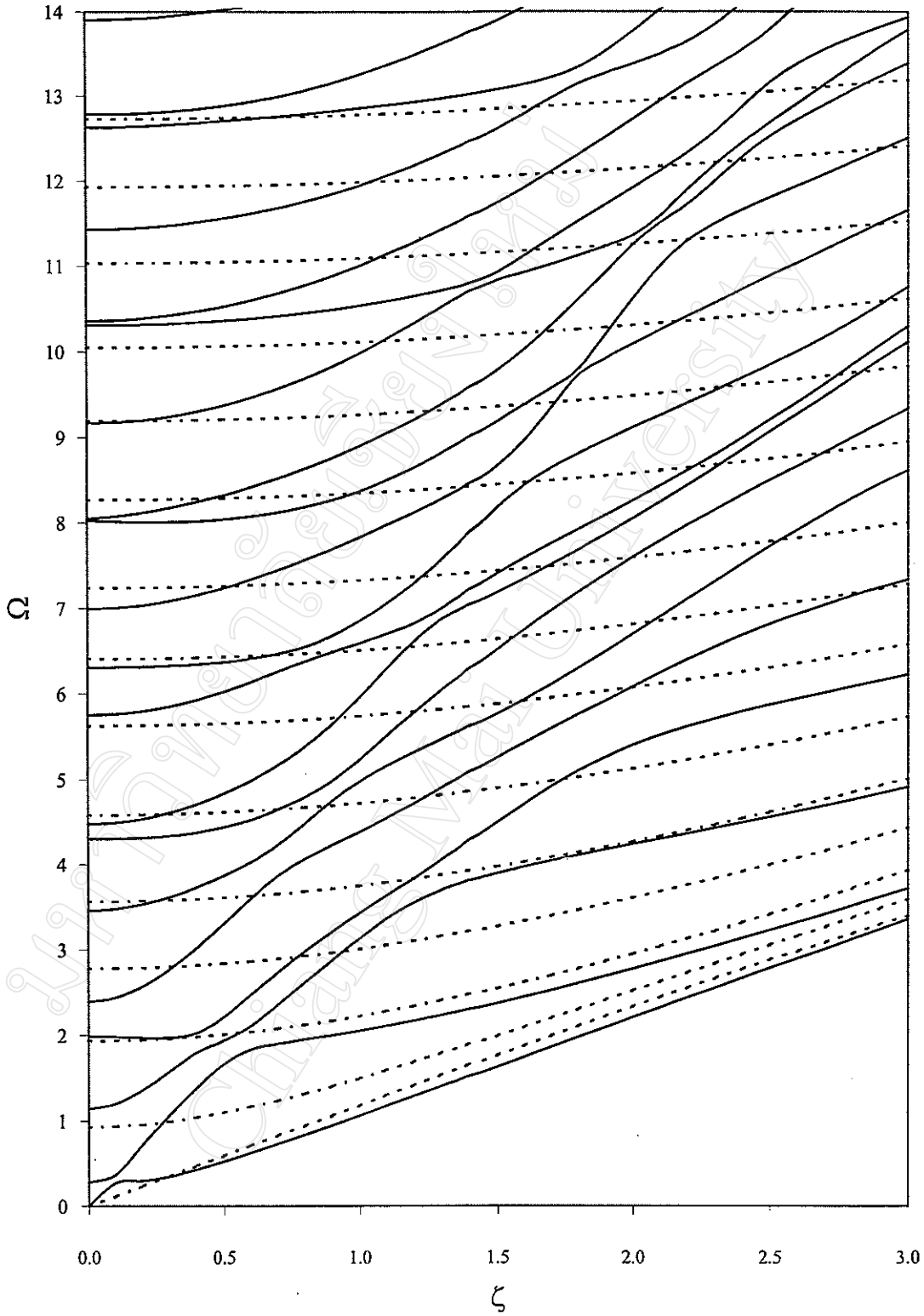

Figure 3.4 Frequency spectrum for a cylinder composed of [Gr/Gl/Gr/Gl] with H/R = 0.5 (—— Longitudinal mode, ----- Torsional mode)

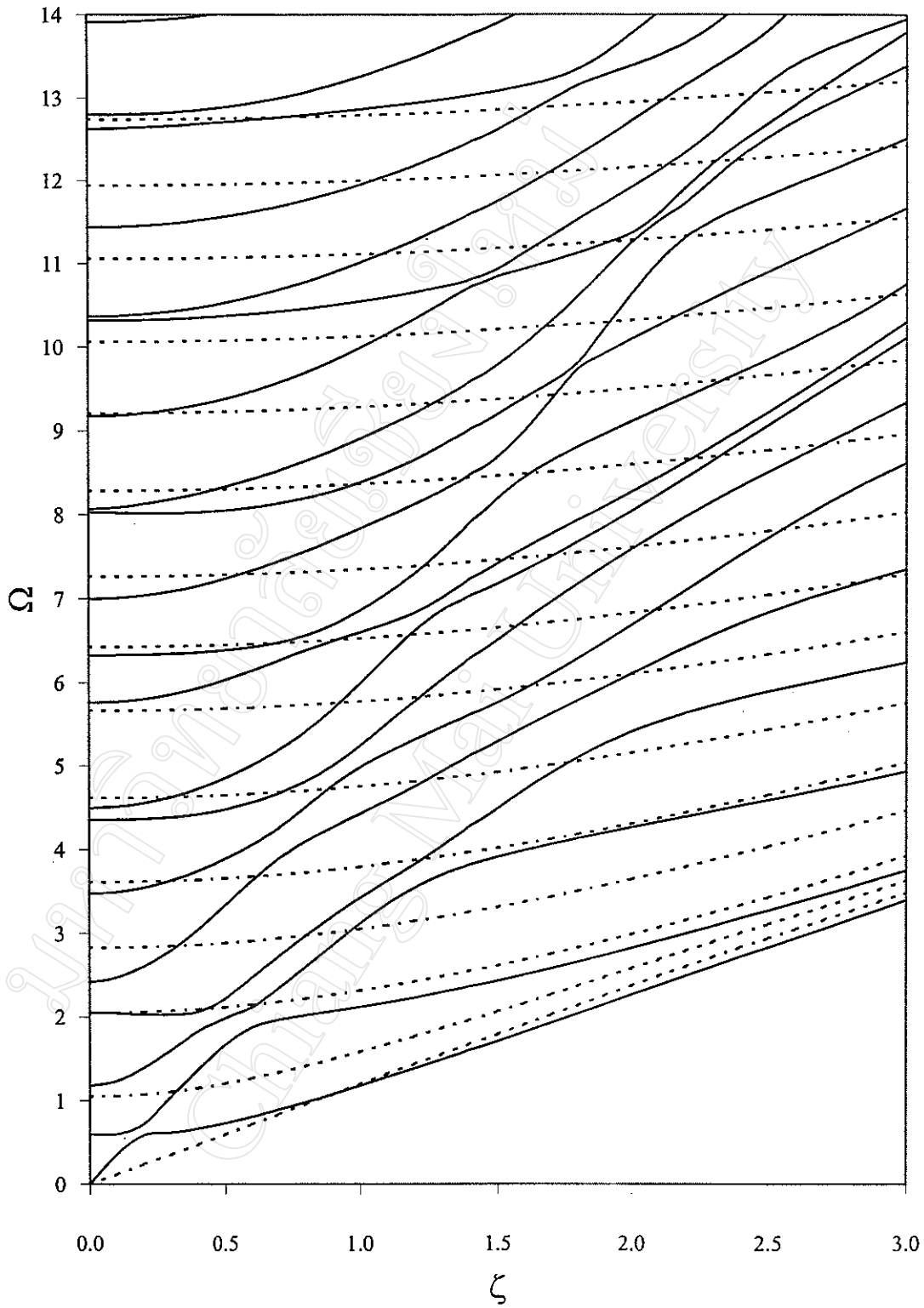

Figure 3.5 Frequency spectrum for a cylinder composed of [Gr/Gl/Gr/Gl] with H/R = 1.0 (—— Longitudinal mode, ----- Torsional mode)

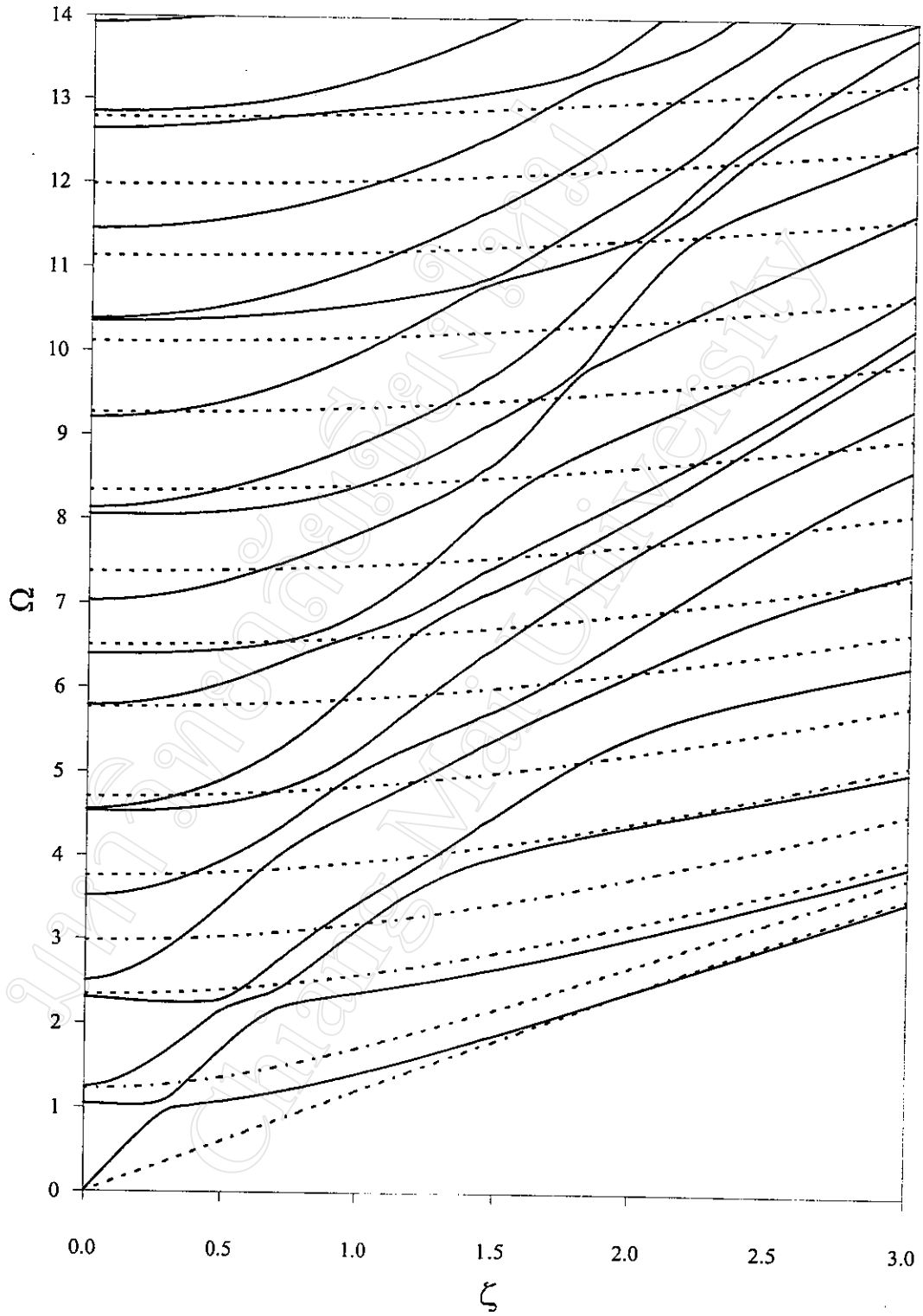

Figure 3.6 Frequency spectrum for a cylinder composed of [Gr/Gl/Gr/Gl] with H/R = 1.5 (—— Longitudinal mode, ----- Torsional mode)

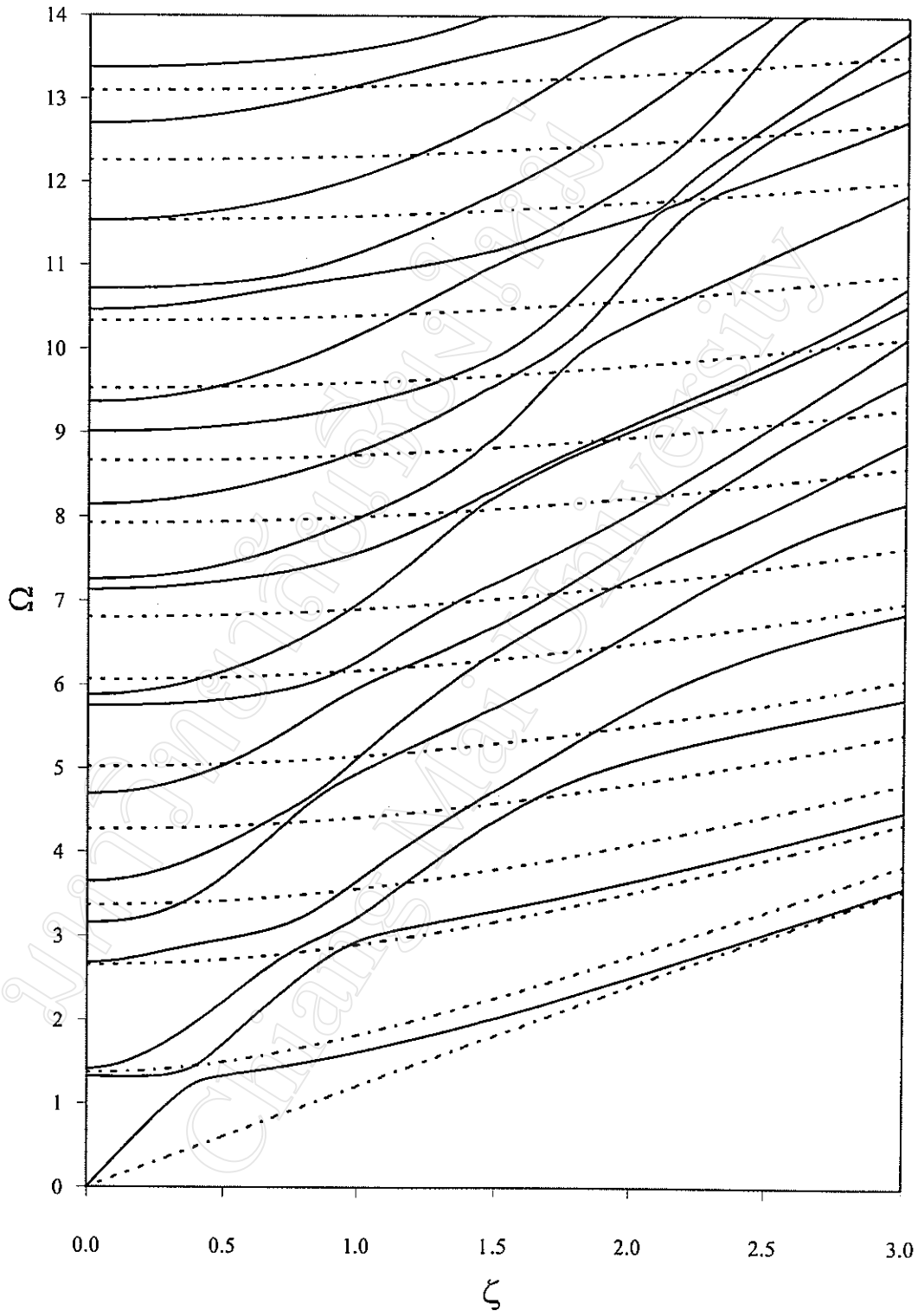

Figure 3.7 Frequency spectrum for a cylinder composed of [Gr/Gl/Gr/Gl] with H/R = 1.9 (—— Longitudinal mode, ----- Torsional mode)

Example 4

Axisymmetric and torsional free vibrations of a ten-layered $[\text{Gr/Gl/Gr/Gl/Gr}]_s$ laminated cylinder with H/R of 1.0 is considered in this example. Subscript s denotes symmetrical layering. In order that the material properties be transversely isotropic, the fiber directions align in the axial direction of the cylinder. The thickness ratio $H^{(Gr)}/H^{(Gl)}$ is the same as that in previous example; i.e. 0.5. The reference frequency and the reference wavenumber are defined, respectively, as:

$$\omega_{ref} = \frac{\pi}{H}\sqrt{\frac{C_{44}^{(Gr)}}{\rho^{(Gr)}}} \; ; \qquad \xi_{ref} = \frac{\pi}{H}.$$

It should be noted that the inner layer is graphite/epoxy. This example demonstrates the applicability of the method for a cylinder consisted of large number of layers.

Figure 3.8 presents the frequency spectrum for both cases of vibration. The displacement variation through the thickness of the cylinder for the first ten modes of axisymmetric vibration at $\zeta = 1.0$ are presented in Figures 3.9. It can be seen from Figure 3.8 that the spectrum has considerably high degree of weak coupling for longitudinal modes. It should be mentioned here that in order to obtain weak coupling roots, caution must be taken during the root scanning process. In any case, if one of the weak coupling roots is missing, the scanning at that particular area needs to be redone with smaller interval.

Figures 3.9 show that the axial motion is insignificant for the first and the second modes while it predominates for the tenth mode. In other modes, however, both motions are coupled.

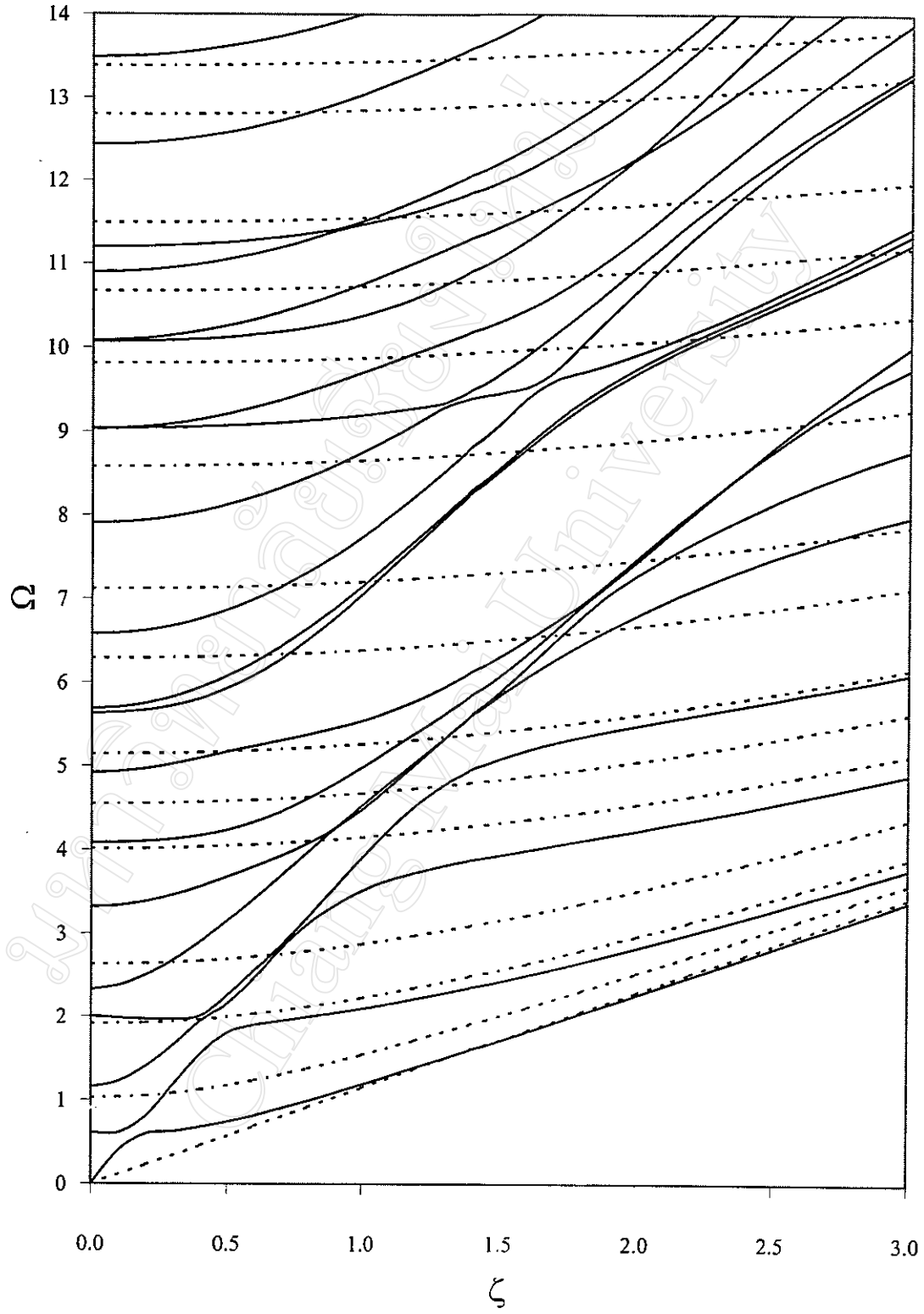

Figure 3.8 Frequency spectrum for a cylinder composed of $[Gr/Gl/Gr/Gl/Gr]_s$ with H/R = 1.0

(—— Longitudinal mode, ----- Torsional mode)

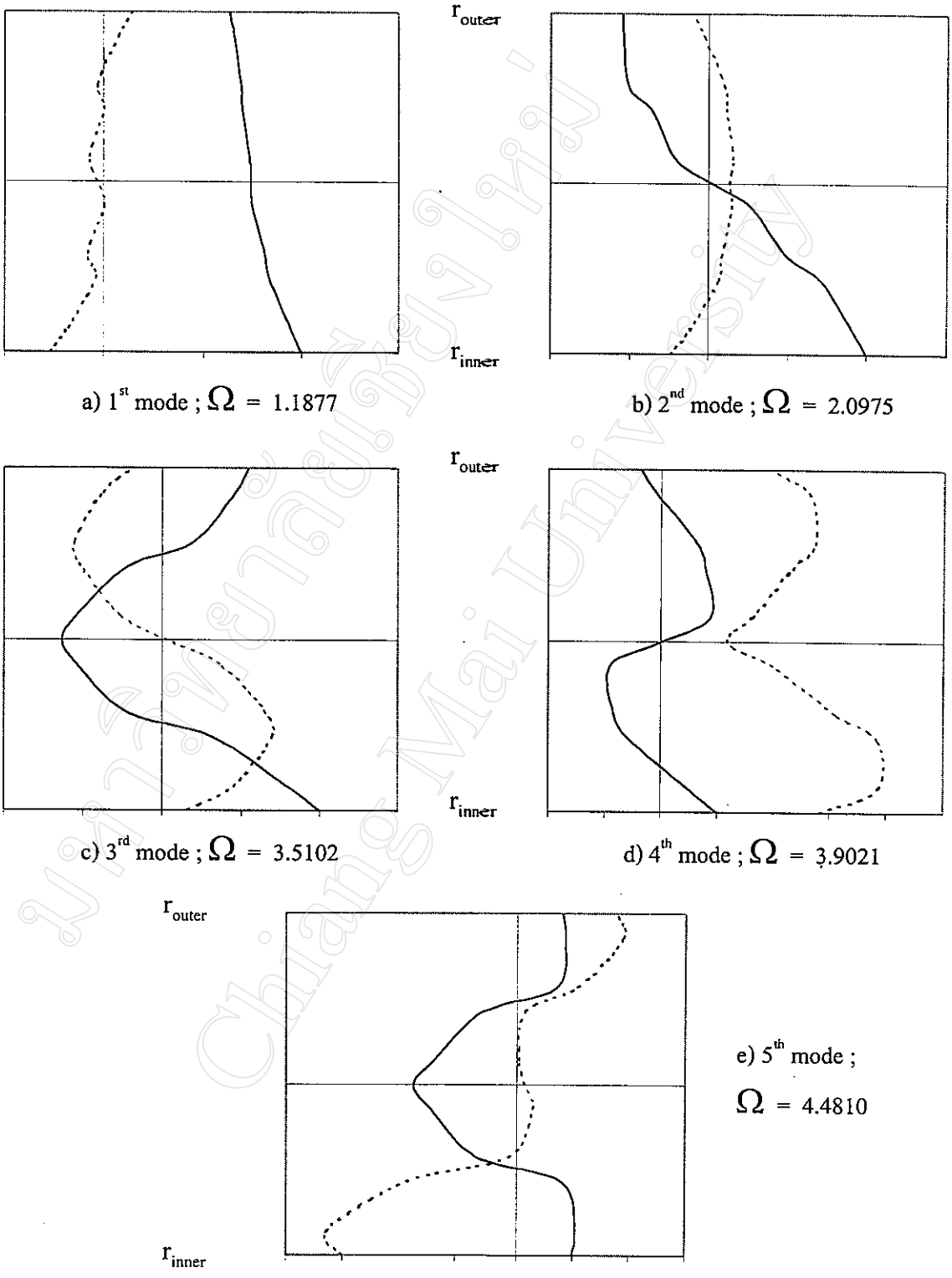

Figure 3.9 Displacement distribution for axisymmetric free vibration of the ten-layered cylinder at ζ of 1.0 (—— u, ----- w)

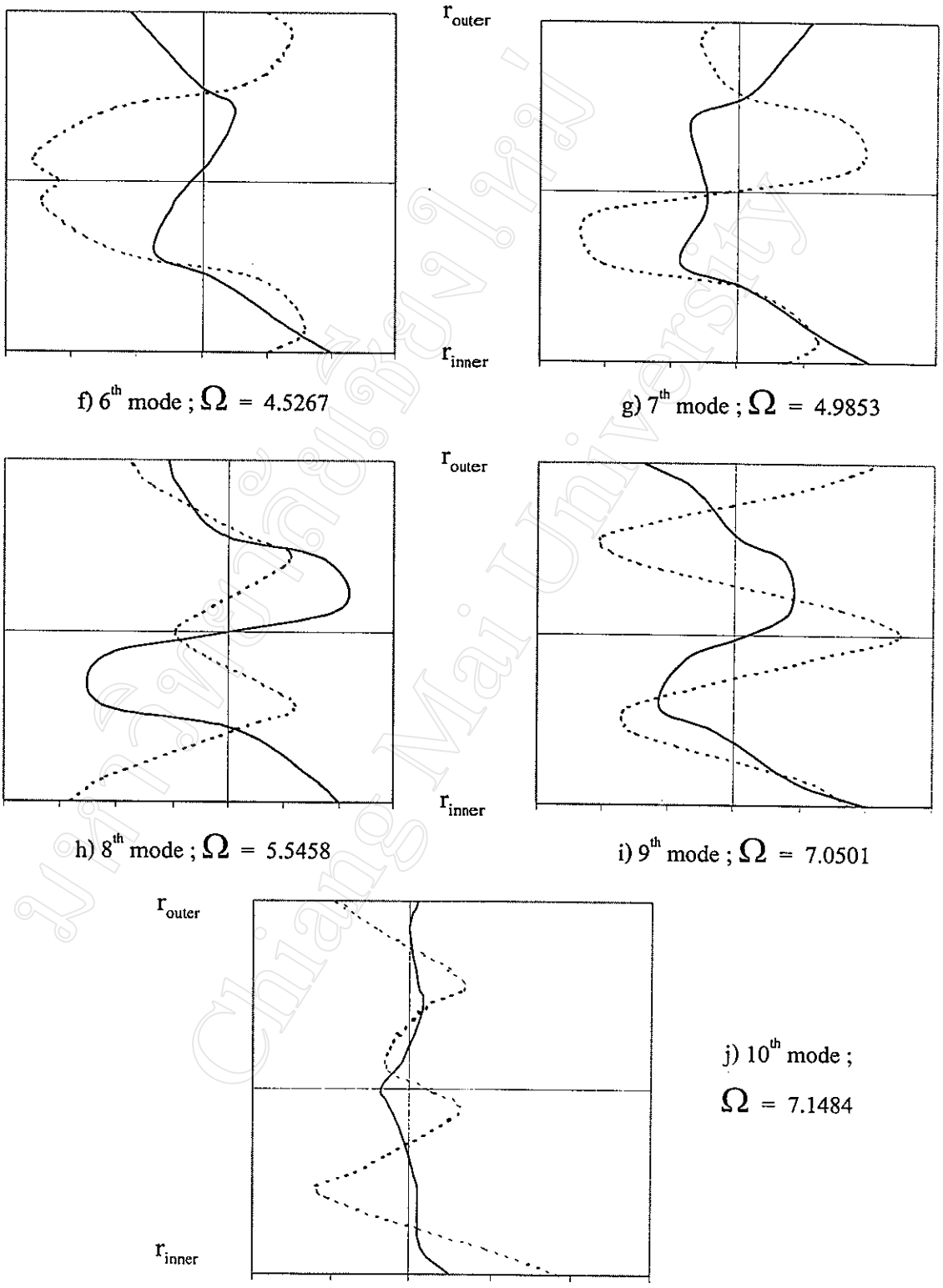

Figure 3.9 (Cont.) Displacement distribution for axisymmetric free vibration of the ten-layered cylinder at ζ of 1.0 (—— u, ----- w)

Example 5

The first two modes axisymmetric vibrations for four laminated cylinders are investigated. The cylinders considered are:

1. A three-layered [Gr/Gl/Gr] cylinder;
2. A four-layered [Gr/Gl/Gr/Gl] cylinder;
3. A six-layered $[Gr/Gl/Gr]_S$ cylinder; and
4. A ten-layered $[Gr/Gl/Gr/Gl/Gr]_S$ cylinder.

All cylinders have the thickness ratio $H^{(Gr)}/H^{(Gl)}$ of 0.5 and the thickness to mean radius ratio H/R of 0.1. The reference frequency and the reference wavenumber are defined, respectively, as:

$$\omega_{ref} = \frac{\pi}{H}\sqrt{\frac{C_{44}^{(Gr)}}{\rho^{(Gr)}}} \quad ; \qquad \xi_{ref} = \frac{\pi}{H}.$$

The objective of this example is to delineate the dispersion characteristics of the first two modes of these four laminated cylinders. In order to accomplish such purpose, the dispersion curves, the plots between normalized frequency and normalized phase velocity c, are presented in lieu of the frequency spectrum. The normalized phase velocity relates the normalized frequency and the normalized wavenumber as

$$c = \frac{\Omega}{\zeta} = \frac{v}{v_{44}^{(Gr)}},$$

where v is the wave velocity and $v_{44}^{(Gr)}$ is the shear wave velocity of graphite/epoxy, Figure 3.10 shows the dispersion curves for all four laminated cylinders. It can be seen from Figure 3.10 that the lowest branches for all four cylinders are almost identical. The wave speed increase with the increasing frequency and reaches a constant normalized velocity. This constant normalized velocity lies in between the normalized shear wave velocity of graphite/epoxy and that of glass/epoxy. The second branches for the four cylinders is quite different. Since the first modes of vibration of the four laminated cylinder is almost identical. Further investigation is carried out to see the possibility of representing laminated cylinders with "equivalent" single-layer cylinders.

Therefore these four laminated cylinders are treated as four "equivalent" single-layer cylinders using the Globally Averaged Stiffness model (Bogdanovich and Deepak, 1997) described in Appendix D. Figure 3.11 shows the dispersion curves of these four "equivalent" single-layer cylinders. It can be seen that the first modes of vibration in the four cylinders are also almost identical. Comparison between Figure 3.10 and Figure 3.11 shows that the lowest modes of vibration in laminated cylinders and those of "equivalent" single-layer cylinders are almost indistinguishable. The discrepancy becomes more noticeable for less number of layers, i.e. 3 layers cylinder.

From the aforementioned discussion, it is suggested that the first mode of vibration should not be used in characterizing material properties for different layered cylinders comprising of same materials.

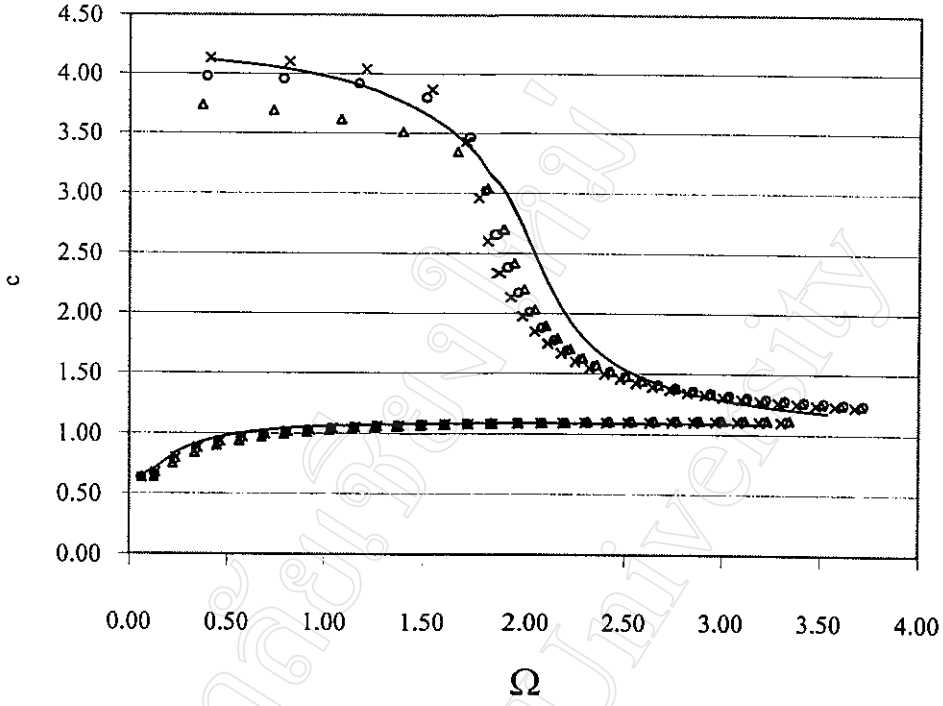

Figure 3.10 Dispersion curves for the four laminated cylinders

(— [Gr/Gl/Gr] , Δ [Gr/Gl/Gr/Gl] , × $[Gr/Gl/Gr]_S$, O $[Gr/Gl/Gr/Gl/Gr]_S$)

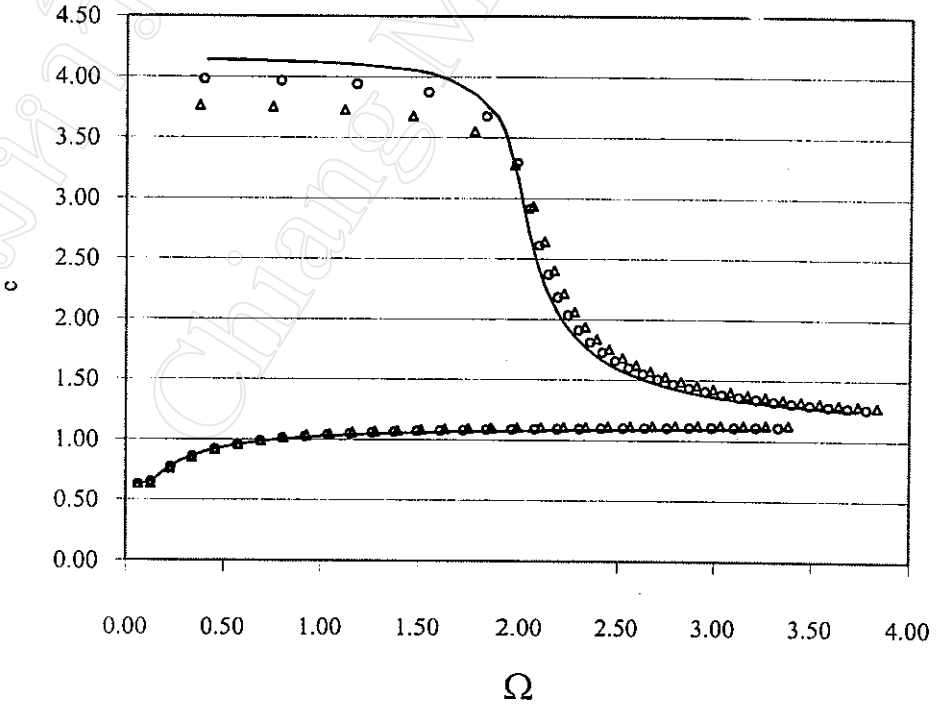

Figure 3.11 Dispersion curves for the four "equivalent" single-layer cylinders

(— [Gr/Gl/Gr] and $[Gr/Gl/Gr]_S$, Δ [Gr/Gl/Gr/Gl] , O $[Gr/Gl/Gr/Gl/Gr]_S$)

3.3 Limitation of the Propagator Matrix Method

Although theoretically it may seem that the propagator matrix method presented in this study can be applied to study free vibration of any transversely isotropic cylinder, numerically the method illustrates some vulnerability. Several attempts have been placed to pin point numerical weakness of the method. It was found that when the value of m lies in the range of 0 and C_{33}, i.e. $0 < m < C_{33}$, the matrix $[D]$ in Eq. (28) contains $I_n(\xi\alpha r)$, $K_n(\xi\alpha r)$, $I_n(\xi\beta r)$, and $K_n(\xi\beta r)$ or $J_n(\xi\alpha r)$, $Y_n(\xi\alpha r)$, $I_n(\xi\beta r)$, and $K_n(\xi\beta r)$, depending on m is less than or more than C_{44}, respectively. When the argument $(\xi\beta r)$ becomes large, i.e. greater than 50, the propagator matrix of the cylinder provides linearly dependent equations. This yields zero determinant of $[P]$ regardless of the value of ξ or ω. Further investigation on the behaviors $e^{-x}I_n(x)$ and $e^{x}K_n(x)$ which are used for high argument of x in the $[D]$ matrix shows that, for high argument of x, i.e. x>50, $e^{-x}I_0(x) \approx e^{-x}I_1(x)$ and $e^{x}K_0(x) \approx e^{x}K_1(x)$. This may be one of the reason that $[P]$ becomes linearly dependent. However, this study is unable to provide a clear explanation of why these high argument behaviors of modified Bessel functions lead the propagator matrix to be linearly dependent.